

Discrete-to-continuum modeling of spider silk fiber composites

Ada Amendola^{*}, Julia de Castro Motta, Fernando Fraternali

Department of Civil Engineering, University of Salerno, Via Giovanni Paolo II, 132 84084 Fisciano (SA), Italy

ARTICLE INFO

Keywords:

Spider silk
Virial stress
Fiber networks
Silk composites

ABSTRACT

This work presents a discrete-to-continuum approach to the constitutive response of composite materials formed by embedding a network of spider silk fibers in a matrix material. A multiscale model that makes use of the virial stress concept of statistical mechanics is formulated, which accounts for hyperelastic constitutive equations of the component materials. The finite element implementation of the given constitutive equations is also carried out. Numerical simulations show the response of a silk composite formed by embedding a spider orb web in a matrix material, and illustrate the main features of the proposed model. In the presence of a weak matrix, the force–displacement response of a silk composite is compared with that deriving from an atomistic modeling of the spider orb web. A simulation of the response of a composite equipped with an elastomeric matrix is also discussed.

1. Introduction

The peculiar mechanical properties of spider silks, and their ability to combine extreme values of lightness, strength, ductility and toughness are extensively documented in the literature (see, e.g., [1–4] and references therein). The radial threads and the terminal supports of the spider orb webs are made of the strong and tough major-ampullate dragline silk, while the spiral threads consist of a more flexible and viscid type of silk, which is well suited to capture preys [4,5]. Other types of silk are produced by different glands of spiders for various purposes, including coating of spiral threads, attachments to substrates, prey wrapping and egg sacs [2]. The outstanding material properties of the dragline silk (tensile strength up to 1.6 GPa, toughness up to 200–400 MJ/m³ [1,6]) mainly derive from the hierarchical architecture of the fibers, which dictates the material mechanical behavior on multiple length scales. A single thread consists of a bundle of microfibrils wrapped in a skin layer, which exhibit diameters ranging from 30 nm to more than 100 nm, and are formed by crystalline β -sheets embedded in a disordered amorphous matrix [3,6,7]. The great energy absorption capacity of spider orb webs has been linked to the breakage of hydrogen bonds and the uncoiling of the chains of proteins forming the silk fibrils, which is referred to as ‘sacrificial bonds and hidden lengths’ (SBHL) mechanism in the literature (see, e.g., [8,9] and references therein).

The design and fabrication of synthetic fibers matching the remarkable mechanical behavior of spider silks represents an open challenge for scientists and materials engineers [2,9,10]. Active lines of research in this field include the artificial spinning of recombinant silk proteins and regenerated silk [2,11,12], as well as the electrospinning of

synthetic polymeric fibers formed by aligned nanofibrils and linking molecules, which combine high strength and high toughness [13]. The development of hybrid composites mixing spider silks with inorganic nanomaterials (e.g., carbon nanotubes) is also receiving increasing attention in the scientific community [14,15]. The additive manufacturing of spiderweb-inspired composite materials obtained by combining an elastomeric matrix with 3D-printed microscale fibers made out of polycarbonated filaments, which are designed so as to reproduce the SBHL mechanism of silk fibrils, has been investigated in [9].

Either discrete or continuous approaches have been proposed to mechanically model the hierarchical structure of spider silks [6,16]. Multiscale approaches have also been frequently employed, making use of either information-passing discrete models [3,16], or microstructure-informed constitutive equations at the continuum level [5,7,17–19]. The present work contributes to such a literature by proposing a novel discrete-to-continuum approach, which is aimed at linking the mechanical response of the individual spider silk threads with that of a continuous medium that incorporates these elements into a matrix phase [14,15]. Such a medium is modeled through a homogenization approach that makes use of the virial stress concept of molecular dynamics at zero temperature [20,21] (Section 2). We restrict our attention to the nonlinear elastic response of the analyzed composites, by addressing a pseudo-elastic modeling of the hysteretic behavior expected under loading-unloading cycles [22,23] to future work. When the matrix material is absent, a distinctive feature of the proposed model is that it predicts a stress field that corresponds to the continuum limit of the force network carried by the silk fibers, provided

^{*} Corresponding author.

E-mail address: adaamendola1@unisa.it (A. Amendola).

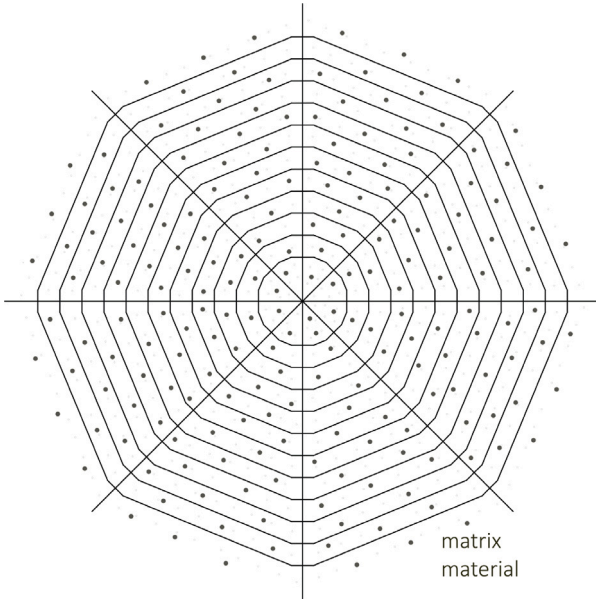


Fig. 1. Reference configuration of a silk fiber network embedded in a matrix material.

that such a network is derived from a structured mesh and matches suitable regularity conditions [24]. We apply the model formulated in Section 2 to the prediction of the mechanical response at the continuum level [25] of an orb web embedded in a matrix material, which is subject to transverse forces [4,5] (Section 4). A first group of numerical results deals with the case of a weak matrix composite, with the aim of approximating the response of a spider web under an impact with a pray through a continuum model. An additional simulation instead analyzes the embedding of a spider web into an elastomeric matrix to form an impact absorption material layer. The results given in Section 4 illustrate the ability of the proposed multiscale approach in bridging the gap between the response at structure-scale of the fiber network and the behavior in the continuum limit of a silk composite. We draw the main conclusions of the present study and directions for future research in Section 5.

2. A discrete-to-continuum constitutive model of a silk composite

Let us consider a network S_w of silk fibers/fibrils embedded in a matrix material, which forms a continuous silk composite B_w at the mesoscale, in two- or three-dimensions (see Fig. 1).

Let \underline{F} denote the deformation gradient of B_w , and let $\underline{C} = \underline{F}^T \underline{F}$ denote the right Cauchy–Green deformation tensor. By focusing our attention on isotropic matrix materials and assuming that the silk threads are loaded in simple tension/compression, we make use of the following invariants of \underline{C} (see, e.g., [26–29]):

$$\begin{aligned} I_1 &= \text{tr}(\underline{C}), \\ I_2 &= \frac{1}{2} [\text{tr}(\underline{C})^2 - \text{tr}(\underline{C}^2)], \\ I_3 &= \det(\underline{C}), \\ I_4^{(i,j)} &= \underline{N}^{(i,j)} \cdot \underline{C} \otimes \underline{N}^{(i,j)} \end{aligned} \quad (1)$$

where $\underline{N}^{(i,j)}$ is the unit vector aligned with the direction of the (i, j) silk thread in the reference configuration (Fig. 2).

We compute the second Piola–Kirchhoff stress tensor \underline{S} of \hat{B}_w through the following additive formula [26–29]:

$$\underline{S} = \underline{S}_m + \underline{S}_f \quad (2)$$

where \underline{S}_m is the stress tensor associated with the matrix material and \underline{S}_f is the stress associated with the silk fiber network. The constitutive

equation for \underline{S}_m is written as follows

$$\underline{S}_m = 2 V_m \frac{\partial W_m}{\partial \underline{C}} \quad (3)$$

where V_m is the volume fraction of the matrix material, and W_m is a given strain energy function of the invariants I_1, I_2, I_3 [26,29].

We now pass to consider the second Piola–Kirchhoff stress tensor \underline{S}_f , which is associated with an averaging volume Ω centered at the generic point of B_w . The latter encompasses an arbitrary collection of silk threads featuring end points (i, j) . We compute \underline{S}_f through the following formula of the virial stress of a molecular system at zero temperature [21,24]:

$$\underline{S}_f = \frac{1}{2|\Omega|} \sum_{i,j} (\underline{X}^{(j)} - \underline{X}^{(i)}) \otimes \hat{\underline{f}}^{(i,j)} \quad (4)$$

Here, $|\Omega|$ is the measure of Ω ; $\hat{\underline{f}}^{(i,j)}$ is the referential description of the axial force carried by the (i, j) silk thread; $\underline{X}^{(i)}$ and $\underline{X}^{(j)}$ are the position vectors of the end points of such a fiber in the reference configuration. Upon setting:

$$\underline{X}^{(j)} - \underline{X}^{(i)} = L^{(i,j)} \underline{N}^{(i,j)}, \quad \hat{\underline{f}}^{(i,j)} = \hat{f}^{(i,j)} \underline{N}^{(i,j)}, \quad (5)$$

where $L^{(i,j)} = \|\underline{X}_j - \underline{X}_i\|$, we can rewrite Eq. (4) as follows:

$$\begin{aligned} \underline{S}_f &= \frac{1}{2|\Omega|} \sum_{i,j} L^{(i,j)} \hat{f}^{(i,j)} \underline{N}^{(i,j)} \otimes \underline{N}^{(i)} \\ &= \frac{1}{2|\Omega|} \sum_{i,j} A^{(i,j)} L^{(i,j)} \frac{1}{\lambda^{(i,j)}} \frac{\partial W^{(i,j)}}{\partial \lambda^{(i,j)}} \underline{N}^{(i,j)} \otimes \underline{N}^{(i,j)} \end{aligned} \quad (6)$$

Here, $A^{(i,j)}$ denotes the nominal cross-section areas of the $i - j$ silk thread; $W^{(i,j)}$ denotes the corresponding strain energy function, and we have set $\lambda^{(i,j)} = \sqrt{I_4^{(i,j)}}$. Eq. (6) suggests that Ω can be regarded as a hyperelastic region endowed with the following strain energy function (see [26], pag. 220):

$$W_\Omega = V_m W_m + \frac{1}{2} \sum_{i,j} V_f^{(i,j)} W^{(i,j)}(\lambda^{(i,j)}). \quad (7)$$

$V_f^{(i,j)}$ denoting the volume fraction of the $i - j$ silk thread within Ω . It is worth observing that the presence of the averaging volume $|\Omega|$ gives a multiscale character to the constitutive Eqs. (6), (7).

3. A finite element model of a silk composite

Let us now introduce the finite element (FE) discretization \hat{B}_w of B_w shown in Fig. 2. We describe the constitutive response of the individual silk threads forming such a model through the multiscale model proposed by De Tommasi et al. in [7]. This model accounts for the following wormlike chain (WLC) law of the stress–strain response of the soft fraction of the material forming the threads (amorphous phase):

$$\sigma_s = \hat{\sigma}_s(\varepsilon, \varepsilon_c) = E_s \left(\frac{1}{4} \left(1 - \frac{\varepsilon}{\varepsilon_c} \right)^{-2} - \frac{1}{4} + \frac{\varepsilon}{\varepsilon_c} \right) \quad (8)$$

where σ_s denotes the nominal stress carried by the soft phase; ε is the engineering strain of the fiber; ε_c is a limit strain (or contour length [7]) and E_s is the Young modulus of the soft phase.

Denoting σ_h the nominal stress carried by the hard, crystalline phase of the thread, the model by De Tommasi et al. [7] assumes:

$$\sigma_h(\varepsilon) = \begin{cases} 0, & \text{if } \varepsilon \leq \varepsilon_a, \\ E_h(\varepsilon - \varepsilon_a), & \text{if } \varepsilon_a < \varepsilon < \varepsilon_t, \\ \sigma_s(\varepsilon, \varepsilon_c), & \text{if } \varepsilon \geq \varepsilon_t, \end{cases} \quad (9)$$

Here, E_h indicates the Young modulus of the hard phase; while ε_a and ε_t denote activation and transition strains, respectively. It is indeed assumed that the hard material is activated for $\varepsilon = \varepsilon_a$ and undergoes a transition to the soft phase for $\varepsilon = \varepsilon_t$. Upon restricting our analysis to

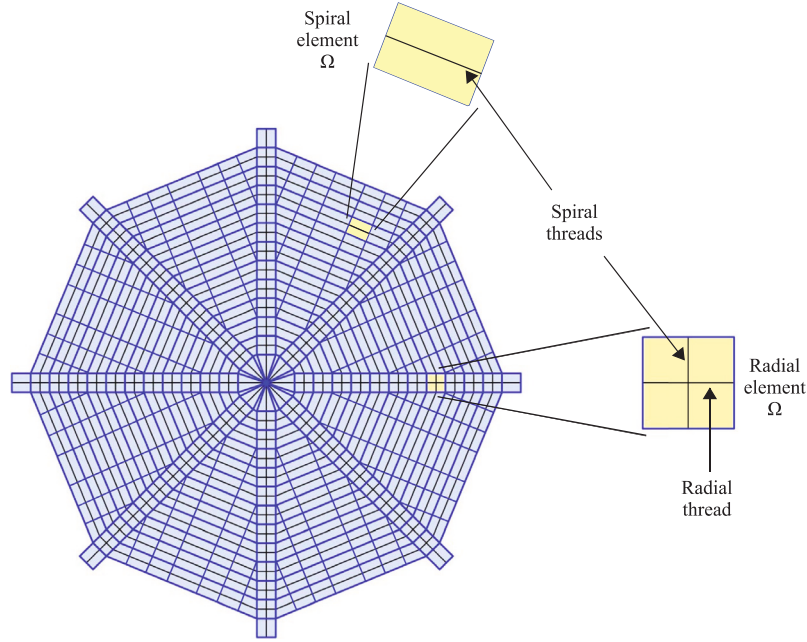


Fig. 2. Finite element model of a composite system formed by embedding a spider orb web into a matrix material.

the loading branch (branch #1) of the stress–strain response, we denote the fraction of the soft material by α and we set:

$$\alpha = \alpha^1(\varepsilon) = \alpha_0 + \int_0^\varepsilon p(\varepsilon_t) d\varepsilon_t, \quad (10)$$

$$\sigma = \sigma^1(\varepsilon) = \alpha^1(\varepsilon) \hat{\sigma}_s(\varepsilon, \hat{\varepsilon}_c(\alpha^1(\varepsilon))) + E_h \left(\int_\varepsilon^\delta p(\varepsilon_t) d\varepsilon_t + \int_{\max(\varepsilon, \delta)}^{\varepsilon+\delta} (\varepsilon - (\varepsilon_t - \delta)) p(\varepsilon_t) d\varepsilon_t \right). \quad (11)$$

where p denotes a Gaussian probability distribution [7].

For what concerns the matrix material, we introduce a nearly incompressible St. Venant - Kirchhoff model described by the following equations [30]:

$$\begin{aligned} W_m &= W_{m,iso} + W_{m,vol}, \\ W_{m,iso} &= \frac{1}{2}(\lambda_m + 2\mu_m)\bar{I}_1^2 - 2\mu_m\bar{I}_2, \\ W_{m,vol} &= \frac{1}{2}k_m(J_{el} - 1)^2, \end{aligned} \quad (12)$$

where λ_m and μ_m are two Lamé constants; k_m is a bulk modulus; \bar{I}_1 and \bar{I}_2 are the first and the second invariant of the isochoric Green–Lagrange strain tensor $\bar{\underline{E}} = \frac{1}{2}(\underline{\bar{C}} - \underline{I})$, respectively. Here, \underline{I} is the identity tensor, and we have set:

$$\underline{\bar{C}} = J_{el}^{-2/3} \underline{C}, \quad (13)$$

$$J_{el} = J/J_{th}, \quad (14)$$

J denoting the determinant of the total deformation gradient tensor, and J_{th} denoting a thermal volume ratio. Assuming that the web is clamped at the boundary, we initially apply a fictitious thermal load to the radial branches (before a mechanical load is applied), in order to model their pretension. Pretension forces play an important role in the stiffness properties of spider orb webs and their magnitude in the webs weaved by different spider species is discussed in [31]. A thermal loading defined by the volume ratio $J_{th} = (1 + \alpha_{m,iso}(T - T_{ref}))^3$ is applied to the radial branches of the finite element model (FEM) shown in Fig. 2, where $\alpha_{m,iso}$ is the coefficient of volumetric thermal expansion of the matrix material, and $T - T_{ref}$ is a suitable temperature change. Due to the end constraints, such a thermal loading produces a radial stress σ_0 at the extremities of the radial branches, and pretension forces $F_0 = \sigma_0 \times h_r \times L_r$, where h_r and L_r denote the thickness and the width of the terminal cross-section, respectively.

4. Numerical simulations

The present section illustrates numerical results obtained through the use of the FEM formulated in the previous section. We examine an orb web imported from Ref. [4], which has an external radius of 0.3927 m. It comprises 8 radial threads, which feature 3.93 μm diameter, and 11 spiral threads, with 2.40 μm diameter. The total mass of the web is 1.97 g.

The constitutive Eqs. (8)–(11) were fitted to the stress–strain response of an atomistically derived model of the *Nephila clavipes* dragline silk presented in [4] (model A), by using the ‘NonlinearModelFit’ command of Mathematica[®] (Version 12.2). Such a fitting procedure led us to estimate $E_s = 183.06$ MPa, $E_h = 875.90$ MPa; $\varepsilon_c = 0.88$; $\delta = \varepsilon_t - \varepsilon_a = 0.60$; $p = 886 e^{-4.5(\varepsilon_t+1)^2}$ (Fig. 3). Upon setting $\lambda = 1 + \varepsilon$, it is easy to recognize that the constitutive model under examination is well described by the following strain energy function:

$$\begin{aligned} W_f &= k (0.324846 (\lambda - 1)^8 - 0.709017 (\lambda - 1)^7 + 0.667853 (\lambda - 1)^6 \\ &\quad - 0.34785 (\lambda - 1)^5 + 0.115503 (\lambda - 1)^4 - 0.0238718 (\lambda - 1)^3 \\ &\quad + 0.00540063 (\lambda - 1)^2) \end{aligned} \quad (15)$$

where $k = 10^5$ MPa.

For what concerns the matrix properties, we prescribe: $k_m = E_m / (3(1 - 2\nu_m))$; $\lambda_m = E_m \nu_m / ((1 + \nu_m)(1 - 2\nu_m))$; $\mu_m = E_m / (2(1 + \nu_m))$; and $\alpha_{m,iso} = -10.6 \times 10^{-4} \text{ } ^\circ\text{C}^{-1}$ [32], where E_m and ν_m are the Young modulus and the Poisson’s ratio of the material, respectively.

The finite element simulations presented hereafter employ two different matrix materials. We initially deal with a continuous model of the spider orb web, which is obtained by embedding such a structure into a fictitious matrix material much weaker than the silk threads. We will refer to this model as ‘weak matrix silk composite’ (WMSC). It exhibits $E_m = E_h \times 10^{-5}$ and $\nu_m = 0.4$. An additional FE simulation considers a cured polydimethylsiloxane silk composite (PDMSC) obtained by embedding the examined spider web into a Sylgard 180 elastomeric matrix [33]. Such a simulation is aimed at studying a fiber composite that can be employed to form an impact absorption material [9]. It employs the matrix properties $E_m = 1.5$ MPa and $\nu_m = 0.45$, which are on the range of values listed in Ref. [33] for Sylgard 180.

The strain energy function of the generic finite element Ω is obtained by making use of Eq. (15) to model the silk threads and Eq. (13)

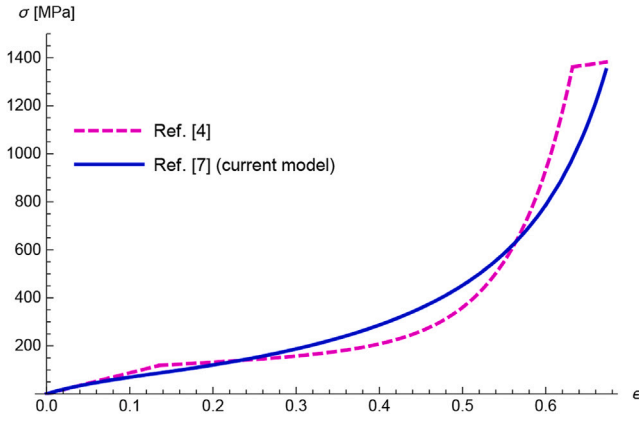
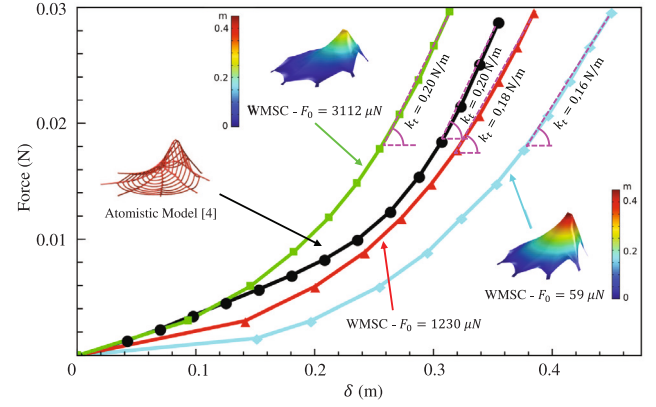


Fig. 3. Fitting of the σ vs. ϵ model by De Tommasi et al. [7] to the stress-strain response atomistically derived by Cranford et al. [4] for the *Nephila clavipes* dragline silk (reproduced with permission).

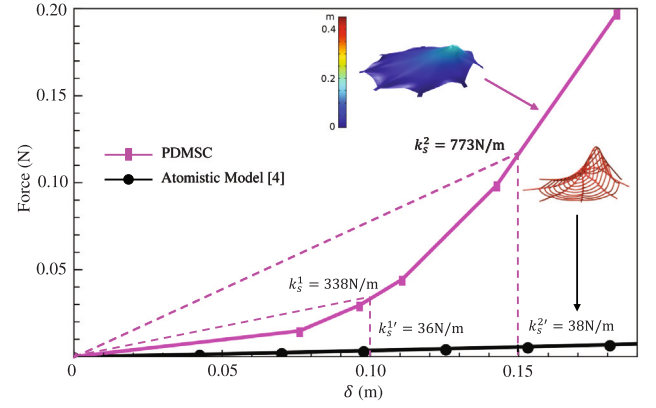
to model the matrix material. The response to a concentrated load F , applied on a radial thread, was simulated through the FE software COMSOL[®] Multiphysics [30], employing a mesh of 488 brick elements and 994 nodes, for a total of 2982 degrees of freedom. The thickness of all the brick elements is equal to $3.93 \mu\text{m}$ (diameter of the radial threads of the spider orb web). A load history that contemplates a transverse force growing linearly from 0 up to a given maximum value F_{max} was applied to a radial node placed at a distance of 0.251 m from the center of the web. A geometrically nonlinear, quasi-static analysis was performed to analyze such a load history through 10 steps, employing the MUMPS solver [30]. The maximum vertical displacement δ was determined at each step of the load history, so as to build the F vs. δ response curve of the system. Figs. 4(a, b) show the responses computed for the analyzed WMSC and PDMSC models.

We run a comparison between the $F - \delta$ curves obtained for the WMSC, for two different values of the pretension force F_0 , and the force-displacement curve predicted by the atomistic model (AM) of the spider web analyzed in [4] (molecular dynamics approach). The examined pretension forces amount to $3112 \mu\text{N}$ ($T - T_{ref} = 270 \text{ }^\circ\text{C}$), $1230 \mu\text{N}$ ($T - T_{ref} = 150 \text{ }^\circ\text{C}$) and $59 \mu\text{N}$ ($T - T_{ref} = 10 \text{ }^\circ\text{C}$). The first two of these pretension forces are in the range of values reported in Ref. [31] for *Nephila* webs (average value: $1.35 \mu\text{N}/\text{mg}$; standard deviation: $\pm 0.97 \mu\text{N}/\text{mg}$). The results shown in Fig. 4(a) demonstrate that the thin membrane model analyzed in this study exhibits a very low effective stiffness coefficient $k_t = dF/d\delta$ against quasi-static transverse loading, when the pretension force F_0 approaches zero. This is clearly visible in Fig. 4(a), where one observes values of k_t that are close to zero for $F_0 = 59 \mu\text{N}$ and $\delta \approx 0$. A significant increase in the stiffness coefficient of the membrane is observed in the large displacement regime, due to second-order effects [34]. Differently, the molecular dynamics modeling presented in [4] for the ‘bare’ spider orb web predicts non-zero transverse stiffness of the web including for small deflections. One observes that the tangent stiffness coefficients of the examined WMSC models well approximate the value of k_t predicted by the AM for $\delta \geq 0.25 \text{ m}$ (see Fig. 4(a)).

Moving on to analyze the response of the PDMSC model, we observe that the $F - \delta$ curve of such a system exhibits a nearly zero stiffness at the origin, due to the absence of pretension forces, as we already observed (Fig. 4(b)). Nevertheless, this curve gets significantly stiffer than those exhibited by the AM of the bare spider web and the WMSC, for $\delta > 0.07 \text{ m}$. When it results $\delta = 0.10 \text{ m}$ and $\delta = 0.15$, the secant stiffness k_s coefficients of the PDMSC (denoted by k_s^1 and k_s^2 in Fig. 4(b), respectively) are nearly ten times and twenty times larger than those exhibited by the bare spider orb web ($k_s^{1'}$ and $k_s^{2'}$). Such results highlight the convenience, in terms of overall



(a)



(b)

Fig. 4. Comparison of force-displacement responses of an atomistic model (AM) of a spider orb web (reproduced with permission from [4]) and FEM simulations of silk composite systems subject to a concentrated transverse load along a radial thread. (a) Comparison between the responses of WMSC and AM models. (b) Comparison between PDMSC and AM responses.

stiffness improvements, of embedding spider web (or spider web-like) fiber networks in elastomeric matrices, with the aim of forming novel composite materials [9].

Fig. 5 illustrates the distributions of the maximum (σ_1) and minimum (σ_3) principal stresses that are associated with the results of the WMSC models shown in Fig. 4(a), in correspondence to the cases with $F_0 = 59 \mu\text{N}$ and $F_0 = 3112 \mu\text{N}$ (minimum and maximum values of the pretension force). For $F_0 = 59 \mu\text{N}$, we observe the occurrence of compressive stresses $\sigma_3 < 0$ over the terminal (clamping) points of the radial elements (stresses absorbed by the supports), and also in correspondence to some annular (or spiral) elements, which are adjacent to the radial branches or close to the center of the membrane (Fig. 5(b)). The compressive stresses assume peak absolute values no greater than 0.05 MPa in annular elements (0.12 MPa under the point load), i.e. extreme values in annular elements equal in magnitude to about 1/10 of the maximum value of the tensile principal stress σ_1 (0.48 MPa, cf. Fig. 5(a)). Such compressive stresses are expected to produce the local wrinkling of the membrane [34–36], whose study is beyond the scope of the present work and is addressed to future research. We note that, for $F_0 = 59 \mu\text{N}$, the spiral compressive stresses σ_3 are significantly reduced in magnitude, as compared to the previous case, and exhibit peak absolute values of the order of 0.015 MPa in annular elements and an absolute value equal to 0.07 MPa under the point

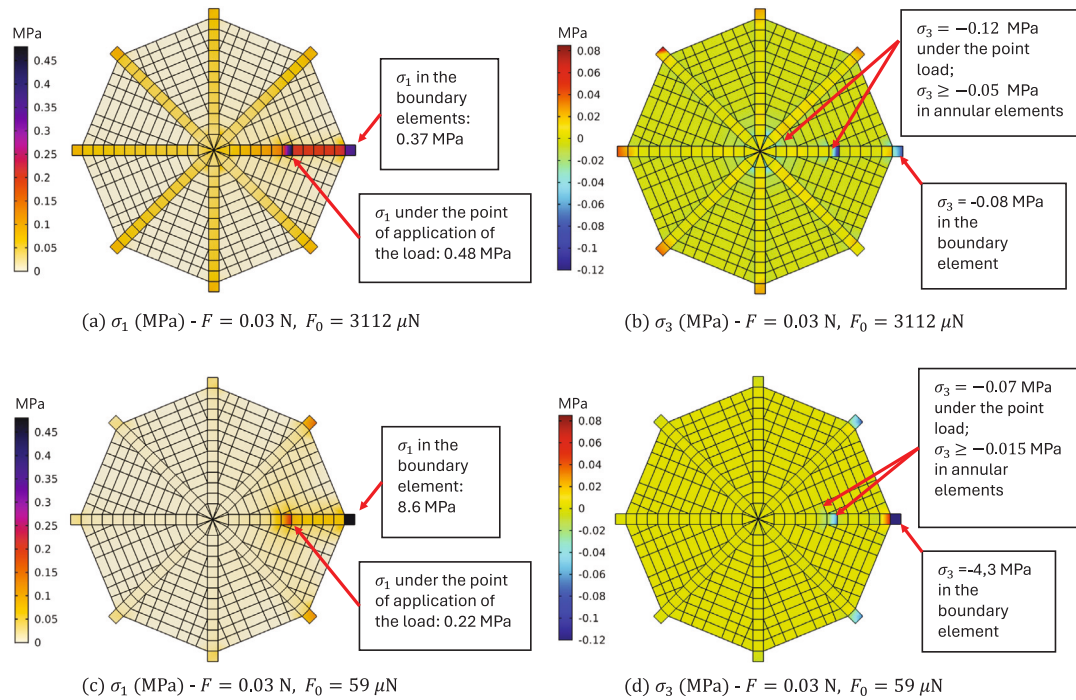


Fig. 5. Maps of the maximum (σ_1) and minimum (σ_3) principal stresses in the WMSC model for $F=0.03$ N and different values of the pretension force F_0 .

load (Fig. 5(d)). The maximum tensile stress σ_1 of the case with the minimum pretension force is nearly equal to 1/2 of the analogous stress value associated with the maximum pretension force (cf. Figs. 5(c) and 5(a)). Such a stress component does not exhibit significantly large negative values, since the lowest values of σ_1 are of the order of -3.5×10^{-4} MPa and -9×10^{-4} MPa for $F_0 = 59$ μ N and $F_0 = 3112$ μ N, respectively. These values are achieved in correspondence to isolated points of the circumferential elements forming the boundary of the membrane. It is worth noting that one can suppress or mitigate the wrinkling of a thin membrane by a number a techniques, which include: boundary reinforcements with cables; metamaterial and/or topology optimization approaches; and the adoption of curved edges, to name but a few examples (refer, e.g., to [36] and references therein).

5. Concluding remarks

We have formulated a discrete-to-continuum approach to the constitutive equation of a composite material that is formed by embedding spider silk threads in a matrix material. The adopted model makes use of the virial stress concept to smear the forces carried by the silk fibers over averaging volumes. Hyperelastic strain energy functions have been introduced to model the elastic response of the matrix material and the reinforcing fibers in the large strain regime. Numerical simulations have highlighted that the presented model is able to reproduce both the response of a bare spider orb web at the continuum level, when combined with a weak matrix material, and the response of a real silk composite. It offers a solid tool to analyze novel composite materials that use recombinant silk, regenerated silk [2,11,12], and/or synthetic and/or 3D-printed polymeric fibers embedded in elastomeric matrices [9,13]. We address an extension of the mechanical model presented in this study to future work, with the aim of including hysteresis effects due to the loading-unloading cycles, via pseudo-elastic approaches [22,23]; to carry out the modeling of the wrinkling phenomenon in thin membranes made of spider silk composites, as well as and to develop suitable techniques for the prevention or mitigation of such a phenomenon [34–36]. Additional lines of future research include the description of strain-rate effects and impact loading, as

well as the application of the given model to a wide range of multiscale fiber-reinforced composites, membrane networks and porous solids [37–39].

CRediT authorship contribution statement

Ada Amendola: Writing – review & editing, Writing – original draft, Project administration, Methodology, Investigation, Funding acquisition, Formal analysis, Conceptualization. **Julia de Castro Motta:** Writing – review & editing, Writing – original draft, Validation, Software, Methodology, Investigation, Formal analysis, Data curation. **Fernando Fraternali:** Writing – review & editing, Writing – original draft, Supervision, Project administration, Methodology, Funding acquisition, Formal analysis, Conceptualization.

Declaration of competing interest

The authors declare that they have no known competing financial interests or personal relationships that could have appeared to influence the work reported in this paper.

Data availability

Data will be made available on request.

Acknowledgments

The authors gratefully acknowledge the great support received by Giacomo Viccione (University of Salerno) in the development of numerical simulations.

Funding

This work was supported by Italian Ministry of University and Research, Italy within the PRIN projects with grant numbers 2022P5R22A, P2022PE8BT and 20224LBXMX (PIs A.A. and F.F. "Ricerca finanziata dall'Unione Europea - Next Generation EU"). A.A. also acknowledges support by the Italian Ministry of Foreign Affairs and International

Cooperation, Italy within the Italy-USA Science and Technology Cooperation Program 2023–2025, Project "Next-generation green structures for natural disaster-proof buildings", grant number US23GR15.

References

- [1] F.G. Omenetto, D.L. Kaplan, New opportunities for an ancient material, *Science* 329 (5991) (2010) 528–531, <http://dx.doi.org/10.1126/science.1188936>.
- [2] L. Eisoldt, A. Smith, T. Scheibel, Decoding the secrets of spider silk, *Mater. Today* 14 (3) (2011) 80–86, [http://dx.doi.org/10.1016/S1369-7021\(11\)70057-8](http://dx.doi.org/10.1016/S1369-7021(11)70057-8).
- [3] G. Xu, L. Gong, Z. Yang, X. Liu, What makes spider silk fibers so strong? From molecular-crystallite network to hierarchical network structures, *Soft Matter* 10 (13) (2014) 2116–2123, <http://dx.doi.org/10.1039/C3SM52845F>.
- [4] S.W. Cranford, A. Tarakanova, N.M. Pugno, M.J. Buehler, Nonlinear material behaviour of spider silk yields robust webs, *Nature* 482 (7383) (2012) 72–76, <http://dx.doi.org/10.1038/nature10739>.
- [5] Y. Jiang, H. Nayeb-Hashemi, Dynamic response of spider orb webs subject to prey impact, *Int. J. Mech. Sci.* 186 (2020) 105899, <http://dx.doi.org/10.1016/j.ijmecsci.2020.105899>.
- [6] F. Fraternali, N. Stehling, A. Amendola, B. Anrango, C.R.C. Holland, Tensegrity modelling and the high toughness of spider dragline silk, *Nanomaterial* 10 (8) (2020) 1–15, <http://dx.doi.org/10.3390/nano10081510>.
- [7] D. De Tommasi, G. Puglisi, G. Saccomandi, Damage, self-healing, and hysteresis in spider silks, *Biophys. J.* 98 (9) (2010) 1941–1948, <http://dx.doi.org/10.1016/j.bpj.2010.01.021>.
- [8] G.E. Fantner, E. Oroudjev, G. Schitter, L.S. Golde, P. Thurner, M.M. Finch, P. Turner, T. Gutschmann, D.E. Morse, H. Hansma, P.K. Hansma, Sacrificial bonds and hidden length: Unraveling molecular mesostructures in tough materials, *Biophys. J.* 90 (4) (2006) 1411–1418, <http://dx.doi.org/10.1529/biophysj.105.069344>.
- [9] S. Zou, D. Theriault, F.P. Gosselin, Spiderweb-inspired, transparent, impact-absorbing composite, *Cell Rep. Phys. Sci.* 1 (11) (2020) <http://dx.doi.org/10.1016/j.xcrp.2020.100240>.
- [10] T. Tenchurin, R. Sharikov, S. Chvalun, Advanced recombinant and regenerated silk materials for medicine and tissue engineering, *Nanotech. Russia* 14 (2019) 290–310, <http://dx.doi.org/10.1134/S1995078019040128>.
- [11] M. Frydrych, A. Greenhalgh, F. Vollrath, Artificial spinning of natural silk threads, *Sci. Rep.* 9 (1) (2019) 15428, <http://dx.doi.org/10.1038/s41598-019-51589-9>.
- [12] L. Valentini, S. Bittolo Bon, M. Tripathi, A. Dalton, N.M. Pugno, Regenerated silk and carbon nanotubes dough as masterbatch for high content filled nanocomposites, *Front. Mater.* 6 (2019) 60, <http://dx.doi.org/10.3389/fmats.2019.00060>.
- [13] X. Liao, M. Dulle, J.M. de Souza e Silva, R.B. Wehrspohn, S. Agarwal, S. Förster, H. Hou, P. Smith, A. Greiner, High strength in combination with high toughness in robust and sustainable polymeric materials, *Science* 366 (6471) (2019) 1376–1379, <http://dx.doi.org/10.1126/science.aay9033>.
- [14] A.P. Kiseleva, G.O. Kiselev, V.O. Nikolaeva, G. Seisenbaeva, V. Kessler, P.V. Krivoschapkin, E.F. Krivoschapkina, Hybrid spider silk with inorganic nanomaterials, *Nanomaterial* 10 (9) (2020) <http://dx.doi.org/10.3390/nano10091853>.
- [15] L. Pan, F. Wang, Y. Cheng, W.R. Leow, Y.-W. Zhang, M. Wang, P. Cai, B. Ji, D. Li, X. Chen, A supertough electro-tendon based on spider silk composites, *Nature Commun.* 11 (1) (2020) 1332, <http://dx.doi.org/10.1038/s41467-020-14988-5>.
- [16] D. López Barreiro, J. Yeo, A. Tarakanova, F.J. Martin-Martinez, M.J. Buehler, Multiscale modeling of silk and silk-based biomaterials—A review, *Macromol. Biosci.* 19 (3) (2019) 1800253, <http://dx.doi.org/10.1002/mabi.201800253>.
- [17] Y. Jiang, H. Nayeb-Hashemi, A new constitutive model for dragline silk, *Int. J. Solids Struct.* 202 (2020) 99–110, <http://dx.doi.org/10.1016/j.ijsolstr.2020.06.007>.
- [18] G. Puglisi, G. Saccomandi, Multi-scale modelling of rubber-like materials and soft tissues: an appraisal, *Proc. Math. Phys. Eng. Sci.* 472 (2187) (2016) 20160060, <http://dx.doi.org/10.1098/rspa.2016.0060>.
- [19] V. Fazio, D. De Tommasi, N.M. Pugno, G. Puglisi, Spider silks mechanics: Predicting humidity and temperature effects, *J. Mech. Phys. Solids* 164 (2022) 104857, <http://dx.doi.org/10.1016/j.jmps.2022.104857>.
- [20] A.K. Subramaniyan, C. Sun, Continuum interpretation of virial stress in molecular simulations, *Int. J. Solids Struct.* 45 (14) (2008) 4340–4346, <http://dx.doi.org/10.1016/j.ijsolstr.2008.03.016>.
- [21] N. Admal, E. Tadmor, A unified interpretation of stress in molecular systems, *J. Elasticity* 100 (2010) 63–143, <http://dx.doi.org/10.1007/s10659-010-9249-6>.
- [22] A. Dorfmann, R. Ogden, A pseudo-elastic model for loading, partial unloading and reloading of particle-reinforced rubber, *Int. J. Solids Struct.* 40 (11) (2003) 2699–2714, [http://dx.doi.org/10.1016/S0020-7683\(03\)00089-1](http://dx.doi.org/10.1016/S0020-7683(03)00089-1).
- [23] A. Dorfmann, R. Ogden, A constitutive model for the Mullins effect with permanent set in particle-reinforced rubber, *Int. J. Solids Struct.* 41 (7) (2004) 1855–1878, <http://dx.doi.org/10.1016/j.ijsolstr.2003.11.014>.
- [24] A. Amendola, On the optimal prediction of the stress field associated with discrete element models, *J. Optim. Theory Appl.* 187 (3) (2020) 613–629, <http://dx.doi.org/10.1007/s10957-019-01572-1>.
- [25] A. Morassi, A. Soler, R. Zaera, A continuum membrane model for small deformations of a spider orb-web, *Mech. Syst. Signal Process* 93 (2017) 610–633, <http://dx.doi.org/10.1016/j.ymsp.2017.02.018>.
- [26] G. Holzapfel, *Nonlinear Solid Mechanics: A Continuum Approach for Engineering*, Wiley & Sons Inc, 2000.
- [27] T.C. Gasser, R.W. Ogden, G.A. Holzapfel, Hyperelastic modelling of arterial layers with distributed collagen fibre orientations, *J. R. Soc. Interface* 3 (6) (2006) 15–35, <http://dx.doi.org/10.1098/rsif.2005.0073>.
- [28] R.W. Ogden, Nonlinear continuum mech. and modeling the elasticity of soft biological tissues with a focus on artery walls, in: *Studies in Mechanobiology, Tissue Eng and Biomaterials*, vol. 20, Springer International Publishing, 2017, pp. 83–156, http://dx.doi.org/10.1007/978-3-319-41475-1_3.
- [29] G. Chagnon, J. Ohayon, J.-L. Martiel, D. Favier, Hyperelasticity modeling for incompressible passive biological tissues, in: *Biomechanics of Living Organs*, in: *Translational Epigenetics*, vol. 1, Academic Press, Oxford, 2017, pp. 3–30, <http://dx.doi.org/10.1016/B978-0-12-804009-6.00001-8>.
- [30] *COMSOL Multiphysics, Structural Mechanics Module - User's Guide*, 2005.
- [31] E. Wirth, F.G. Barth, Forces in the spider orb web, *J. Comp. Physiol. A* 171 (3) (1992) 359–371, <http://dx.doi.org/10.1007/BF00223966>.
- [32] D. Saravanan, Spider silk - structure, properties and spinning, *J. Text. App. Tech. Manag.* 5 (1) (2006).
- [33] I.D. Johnston, D.K. McCluskey, C.K. Tan, M.C. Tracey, Mechanical characterization of bulk Sylgard 184 for microfluidics and microengineering, *J. Micromech. Microeng.* 24 (3) (2014) 035017, <http://dx.doi.org/10.1088/0960-1317/24/3/035017>.
- [34] E. Puntel, L. Deseri, E. Fried, Wrinkling of a stretched thin sheet, *J. Elasticity* 105 (2011) 137–170, <http://dx.doi.org/10.1007/s10659-010-9290-5>.
- [35] Y. Luo, J. Xing, Z. Kang, J. Zhan, M. Li, Uncertainty of membrane wrinkling behaviors considering initial thickness imperfections, *Int. J. Solids Struct.* 191 (2020) 264–277, <http://dx.doi.org/10.1016/j.ijsolstr.2020.01.022>.
- [36] M. Li, K. Zhu, G. Qi, Z. Kang, Y. Luo, Wrinkled and wrinkle-free membranes, *Internat. J. Engrg. Sci.* 167 (2021) 103526, <http://dx.doi.org/10.1016/j.ijengsci.2021.103526>.
- [37] A. Amendola, J. de Castro Motta, G. Saccomandi, L. Vergori, A constitutive model for transversely isotropic dispersive materials, *Proc. R. Soc. Lond. Ser. A Math. Phys. Eng. Sci.* 480 (2281) (2024) 20230374, <http://dx.doi.org/10.1098/rspa.2023.0374>.
- [38] F. Fraternali, C.D. Lorenz, G. Marcelli, On the estimation of the curvatures and bending rigidity of membrane networks via a local maximum-entropy approach, *J. Comput. Phys.* 231 (2) (2012) 528–540, <http://dx.doi.org/10.1016/j.jcp.2011.09.017>.
- [39] J. de Castro Motta, V. Zampoli, S. Chiriță, M. Ciarletta, On the structural stability for a model of mixture of porous solids, *Math. Methods Appl. Sci.* (2023) <http://dx.doi.org/10.1002/mma.9825>.